XX IMEKO World Congress
Metrology for Green Growth
September 9–14, 2012, Busan, Republic of Korea

INVESTIGATION OF FLOW FIELDS IN SONIC NOZZLES FOR METERING SMALL FLOW RATES

E. von Lavante, J. Allofs, and H. Kaya
University of Duisburg-Essen, Germany, Lotharstr. 1, D-43053 Duisburg
R. Kramer, and B. Mickan
Physikalisch-Technische Bundesanstalt (PTB), Germany

Abstract: Due to their long term stability, well understood flow behaviour and very low uncertainty, standard critical flow Venturi nozzles (CFVN) are enjoying great popularity as a calibration tool and flow metering device. Their application to very small flow rates beyond the ISO 9300 Standard, however, leaves many questions unanswered. The present work aimed at detailed description of flow fields within CFVNs of diameters between 15 μm and 80 μm. The present numerical flow simulations were validated by corresponding experimental work.

Keywords: critical flow Venturi nozzles, numerical flow simulation, micro flow rates

1. INTRODUCTION

The use of sonic nozzles in metrology, including the application range and shape of the nozzles, is regulated by the standard ISO 9300 [1]. According to this standard, the validity range of the employment of CFVNs is limited to Reynolds numbers between 10^5 and 10^7. Many times, however, it is desirable to use nozzles at much smaller Reynolds numbers, either for applications with very small volumetric flow rates or for metering gases at very small pressures. In these cases, several investigators [2, 3, 4] have discovered flow effects that were inconsistent with the standard ISO 9300. These included variation of the discharge coefficient C_D as a function of the nozzle back pressure not explainable by the theory offered in ISO 9300, occurence of instabilities and temporary unchoking of the nozzle. After calibration, however, the same nozzles still offer very reliable means of gas metering. The application range of the CFVNs can be extended beyond the ISO 9300 since the nozzles of the standard shape can be manufactured for throat diameters as low as 80 μm. By lowering the exit pressure well below the values recommended by ISO 9300, they can be still reliably operated, resulting in volumetric flow rates down to Q_V = 100 cm^3/min . For even smaller flow rates down to approximately Q_V = 5 cm^3/min, nozzles of throat diameters as small as d_{throat} = 15 μm must be manufactured using simplified shapes. The present nozzle shapes will be discussed in the next chapter.

These extremely small sonic Venturi nozzles still possess the same basic advantages of their larger counterparts. They represent a robust, consistent, simple and reliable means of metering gases and, after proper calibration, are potentially highly accurate. Their practical application to the determination of small flow rates and the generation of gas mixtures on micro scales has been demonstrated by Kramer, Mickan and Schmidt [5]. Here, the very small CFVNs were calibrated using laminar flow elements (LFE) and used singly as well as in series, providing a transfer standard of low uncertainty and high reliability.

The good experience made by the present authors as well as many other investigators with small sonic nozzles employed in metrology justified further study of the corresponding flow fields. It was hoped to gain more detailed knowledge of the behavior of these nozzles when applied to meter small mass flows. This, in turn, should make an explanation of most of the unusual effects occuring in these configurations possible.

With this motivation in mind, the present authors undertook an experimental and numerical investigation of air flow in sonic micro-nozzles, characterized by extremely small Reynolds numbers given by nozzle diameters in the range of 15 – 80 μm. From the very start of the present numerical flow investigation, it was decided to use the flow simulation program ACHIEVE developed by the first author. This program ensured the necessary accuracy in time and space that were essential for the present low Reynolds number potentially unsteady flows. The results obtained by the present numerical flow simulation (computational fluid dynamics, CFD) were validated in several critical cases by the corresponding experimental work performed at the PTB. The close cooperation between the experimental and numerical parts of this study was of advantage when explaining some of the physical phenomena occuring in these nozzles.

2. DISCRIPTION OF THE CASES STUDIED

In the present work, CFVNs of simplified shapes were investigated by numerical flow simulation and experimental flow rate determination having following throat diameters: 15, 25, 35, 50 and 80 μm. The flow in these nozzles was simulated for two exit pressure ratios: p_2/p_0 = 0.4 and 0.3. The nozzles were operated in their forward flow direction (FW), in Fig. 1 from left to right, and their backward

direction, in Fig. from right to left. In addition to the so called "punched" nozzle design (case a in Fig. 1) , so called "drilled" nozzles (case b in Fig. 1) of 25 µm diameter were investigated.

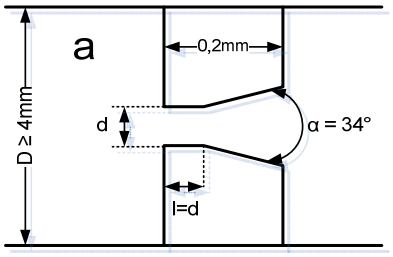

Fig. 1 a: Punched shape of the present nozzles

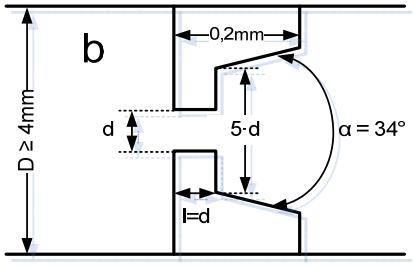

Fig. 1 b: Drilled shape of the present nozzle

A REM photograph of one of the punched nozzles with the diameter of 35 µm can be seen in Fig. 2, as given in [2].

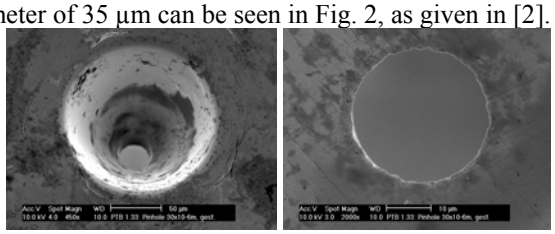

Fig. 2: REM photograph of a nozzle shape a

In all cases the gas being metered was air at atmospheric conditions at the inflow, representing also total pressure and temperature as the pipe supplying the air was much larger than the nozzle diameter. The Reynolds numbers corresponding to the above cases ranged from Re = 193 (d_{throat} = 15 µm) to Re = 1030 (d_{throat} = 80 µm). Clearly, in all cases the flow was laminar. Having high speed flow in very small configurations, it is important to determine if the flow can still be considered as continuum. The non-dimensional number characterizing the type of flow (continuum – rarified gas) is the Knudsen number, defined as Kn = λ/L, where λ is the molecular mean free path and L a global reference length, in this case the throat diameter. Alternatively, the Knudsen number can be computed from [6]:

$$Kn = 1,28 \cdot \sqrt{\kappa} \cdot \frac{Ma}{\mathrm{Re}} \qquad (1)$$

Using equation (1), and substituting the present Reynolds numbers, the Knudsen numbers are:

Kn = 0.008 (d_{throat} = 15 µm)

Kn = 0.0022 (d_{throat} = 80 µm)

The limiting condition for the existence of continuum fluid is Kn < 0.01, indicating that the smallest nozzle was very close to the limit of continuum mechanics.

The very low Reynolds numbers indicated that the flow was laminar with the viscous effects dominating. Consequently, the numerical flow simulations had to be carried out using a method that displayed very low numerical dissipation, yet was still stable for very large flow gradients within the nozzle throat and was capable of accurately capturing the compressible effects in the flow field. Additionally, the method should have been time accurate, as there were possibly high frequency unsteady effects present. To the knowledge of the present authors, no major commercial program possesses the above capabilities, implying that the present investigators had to revert to the code named ACHIEVE, developed by, among others, the first author. The numerical details of the program ACHIEVE can be obtained from Zeitz [7]. The program was fully parallelized using domain decomposition, working with block structured grids. Reasonable computational efficiency was achieved by multi-stage time stepping with optimized Runge-Kutta coefficients.

The numerical grid generation was accomplished using an elliptic grid generation program developed by the first author and subsequently refined by Allofs [8]. The grids had to offer very high resolution of the high flow gradients at the in- and outflow corners of the throat, resulting in between 20,000 and 40,000 cells in the two-dimensional axially symmetric computations. The quality of grids was essential for obtaining feasible results from the numerical flow simulations.

3. EXPERIMENTAL SETUP, THEORY OF OPERATION

The experimental work used for validation of the present numerical simulations was performed at the PTB. By using high resolution digital barometer as a pressure sensor, very sensitive measurement of intake pressure was possible. During the investigations, the flow rate given by the nozzle was measured by a laminar flow element, installed directly in front of the nozzle. The element used in the present work displayed good repeatability and reproducibility. The repeatability was 0.01 ml/min. Downstream of the nozzle, a control valve and a vacuum pump were installed. The control valve was designed for a very wide flow range. It allowed the stabilization of the pressure at the nozzle outflow resulting in fluctuations smaller than 1 mbar. During the investigation, the observed changes of atmospheric pressure were smaller than 0.05 mbar; hence no corrections of the input pressure were necessary. The flow rate determined by the nozzles was measured in both installation directions 5 times, beginning at the lowest output pressure. For the same pressure ratios, no differences in the readouts were observed, meaning that no shift of the LFE occurred.

The presently employed LFE was calibrated using a piston prover shown in Fig. 3. A new type of piston prover using an actively moved piston was developed for particularly low flow rates. The system allowed the calibration transfer

standards like MFE or LFE as well as micro nozzles with an uncertainty of U = 0.05% (k = 2).

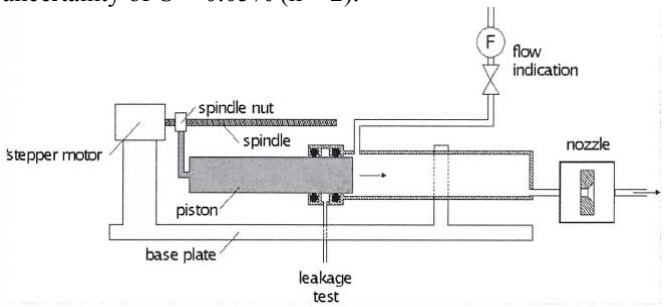

Fig. 3: Schematic picture of the piston prover.

In order to match the flow rate generated by the piston prover to the flow rate determined by a critical nozzle, very stable and sensitive adjustment of the revolution speed of the driving motor was necessary. Adequate properties were achieved by using a stepping motor system. The stepper motor allowed 10 000 steps per rotation. The speed of revolution was changeable by 1 step/rotation.

The flow indication instrument at the intake of the facility was used only for the above mentioned matching of the flow rates. During the calibration, the input valve was closed. If the flow rate of the nozzle and the piston prover were not exactly equal, a slow change of input pressure of the nozzle could be observed. A correction algorithm, taking volume and pressure changes into consideration, allowed achieving the claimed uncertainties even if small pressure changes occured during the calibration.

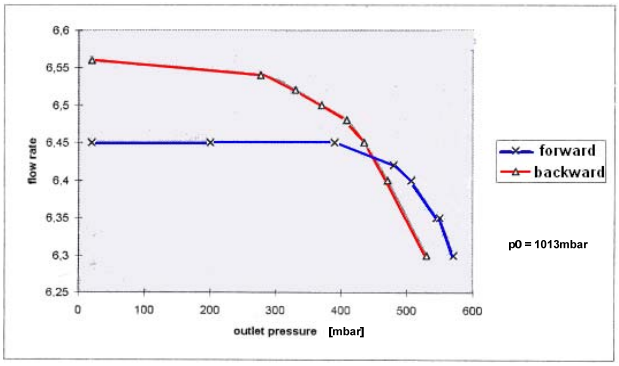

Fig. 4: Experimentally determined flow rate in cm^3/min, (d_{throat} = 35 µm)

Fig. 4 displays the experimentally determined flow rate in the d_{throat} = 35 µm nozzle operated in both directions. As already pointed out in [2], the nozzle in the FW orientation was obviously choked, whereas the BW operated nozzle seems to be unchoked.

According to classical theory which, at first, assumes quasi-one-dimensional flow in the nozzle, the critical mass flow rate is obtained from:

$$\dot{m}_{ideal} = A_{throat} \cdot a^* \cdot \rho^* = A_{throat} \cdot \frac{p_0}{\sqrt{RT_0}} \cdot \psi_r \qquad (2)$$

where a^* is the critical speed of sound, P_0 and T_0 are the total pressure and temperature, respectively, and Ψ is the critical flow function for real gas. The flow rate in real nozzle is different, however, due to boundary layer displacement and two-dimensional effects. It is, therefore, corrected by a so called discharge coefficient C_D:

$$\dot{m}_{real} = c_D \cdot A_{throat} \cdot \frac{p_0}{\sqrt{RT_0}} \cdot \psi_r \qquad (3)$$

Equation (3) is generally used for the determination of the mass flow rate in CFVNs, the discharge coefficient being of great importance. Most of the investigations of CFVNs aim, therefore, at accurate computation or prediction of the discharge coefficient.

4. RESULTS

The combination of most of the above introduced geometries with the two exit pressures resulted in a matrix of 24 cases that were numerically simulated and consequently studied. They are displayed in Table 1. Several interesting facts were observed. All 24 cases considered here were unsteady, with high frequency pressure fluctuations downstream of the nozzle. The frequency ranged between approximately 300 kHz and 1 MHz, with amplitudes of mass flow fluctuation between 0.03% (basically steady) and 9% (fully unsteady with periodic unchoking). There were at least two different mechanisms behind the unsteady mass flow behaviour: in the cases where the throat was always critical, the sonic line was moving streamwise depending on the changing back pressure, where, on the other hand, in the cases with temporary unchoking of the throat flow, the flow function was changing. At the exit pressure ratio of p_2/p_0 = 0.3, all the simulated cases were choked at all times; at p_2/p_0 = 0.4, all the cases were temporary subcritical.

throat diameter [µm]	Reynolds No. Re_d	B.L. thickness δ in [µm]	ratio δ/d	Knudsen number Kn
15	197	5,348	0,3565	0,0153
25	328	6,904	0,2762	0,0092
35	459	8,169	0,2334	0,0066
50	656	9,764	0,1953	0,0046
80	1049	12,351	0,1544	0,0029

Table 1: Summary of simulated cases with the corresponding flow parameters

In Table 1, the cases presently simulated have been summarized. Obviously, as the throat diameter is increased, the Reynolds number Re_D also increases, with the corresponding decrease of the ratio of boundary layer thickness in the throat δ to the throat diameter d, δ/d. This is a clear indication that the influence of the boundary layer is becoming smaller with increasing size of the nozzle, as expected. Particularly in the case of the smallest nozzle with d = 15 µm, the boundary layer forms more than 35% of the throat radial distance (and, of course, even more of the critical area). The Knudsen number is in all cases smaller than 0.1, indicating that the concept of continuum can be applied.

Exemplary for all cases, the flow fields in the 25 µm nozzle will be shown. In the forward orientation, the flow rate

obtained by numerical simulation for $p_2/p_0 = 0.4$ can be seen in Fig. 5.

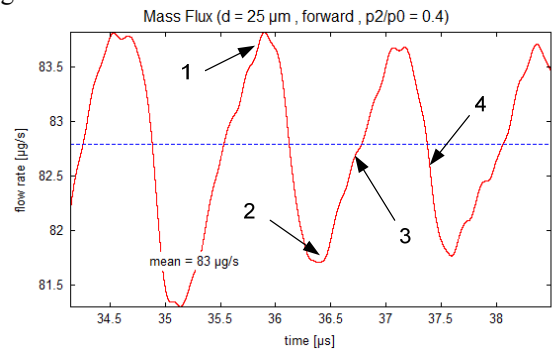

Fig. 5: Computed mass flow rate, $d_{throat} = 25$ µm, forward oriented nozzle

The numbers 1 – 4 in Fig. 5 denote the maximum, minimum, increasing and decreasing flow rates. The corresponding flow fields as Mach number contours are displayed for the same conditions in Fig. 6. Observing that the sonic line is associated with the dark red color (see top bar), its movement in axial direction can be appreciated. The flow at point 2, in particular, corresponded to a subcritical condition in the throat, resulting in a mass flow minimum.

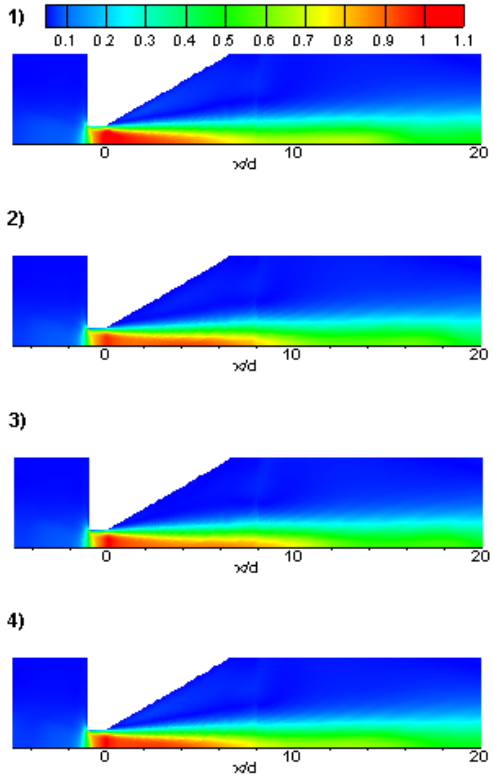

Figure 6: Mach number contours in forward direction, $d_{throat} = 25$ µm, $p_2/p_0 = 0.4$

The flow field in the same nozzle including the streamlines can be seen in Fig. 7. Particularly interesting is the entrainment of the central jet, increasing its size and inducing recirculation in the outflow region. At the same pressure ratio, the backward orientation of the flow results in much larger flow rate fluctuations, with frequent subcritical flow conditions, as seen below.

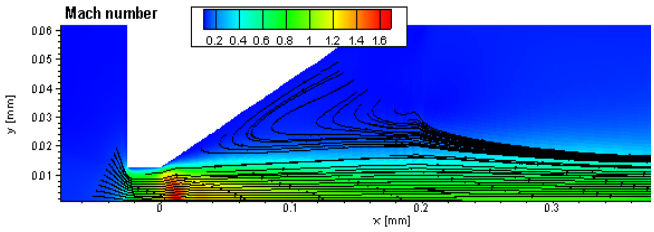

Figure 7: Detailed view of the flow field in $d_{throat} = 25$ µm nozzle

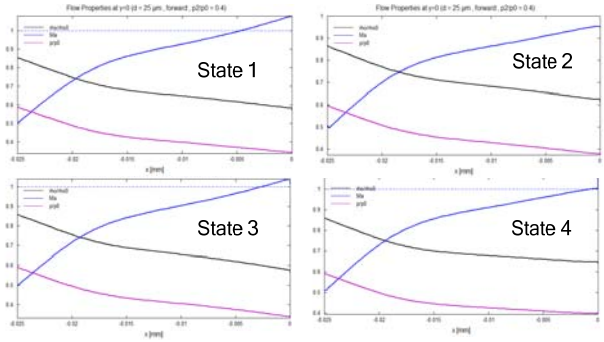

Figure 8: Evolution of the flow variables ρ, M and p

The evolution of density ρ, static pressure p and the local Mach number M through the cylindrical throat region is displayed for the same case in Fig. 8. The horizontal dashed line denotes the critical Mach number M = 1. It is interesting to note that in the state 2, the critical condition was never reached. The states 1-4 differ in the location at which M = 1 was attained, explaining the changes in the mass flow.

At the pressure ratio of $p_{out}/p_0 = 0.3$, the nozzle never unchoked and the Mach number in the throat remained for all 4 states above 1. The flow field was otherwise very similar to Fig. 6 and will not be repeated here.

In Fig. 10, the flow fields in the backward oriented nozzle are shown. The penetration of the jet was somewhat larger as compared to the forward oriented nozzle, in particular at states 2 and 4. Although the boundary layer in the throat area has swept a longer distance along the wall, it was thinner than in the forward nozzle. This can be explained by the flow separation at the entrance corner and the subsequent thickening of the boundary layer.

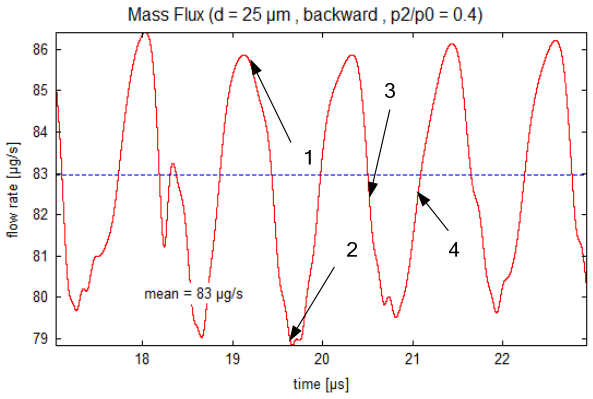

Figure 9: Computed mass flow rate, $d_{throat} = 25$ µm, backward oriented nozzle

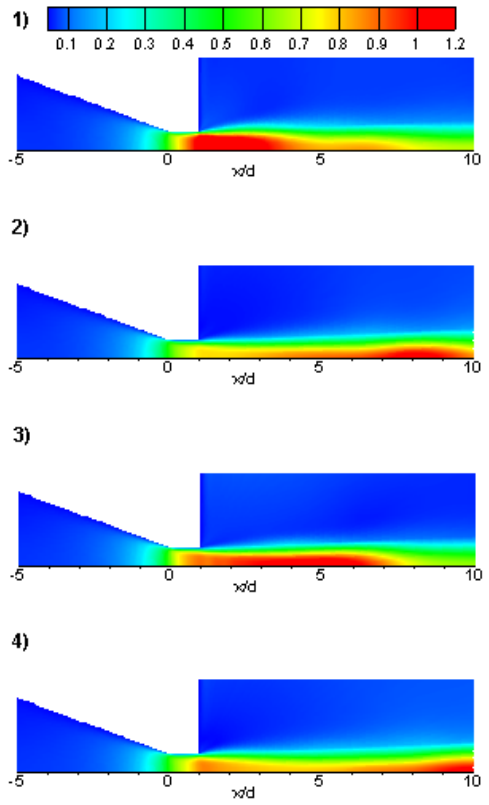

Figure 10: Mach number contours in backward direction, d_{throat} = 25 µm, p_2/p_0 = 0.4

The evolution of the flow variables density, static pressure and Mach number can be seen in Fig. 11.

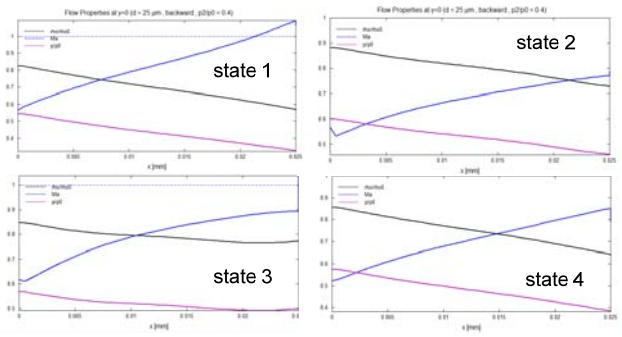

Figure 11: Evolution of the flow variables ρ, M and p Backward oriented nozzle

Interestingly, only at state 1 was the critical Mach number reached, all the other states being subcritical. This explains the lower mass flow for the backward oriented nozzle, although its boundary layer was thinner than in the forward oriented nozzle.

The behavior of the flow in the nozzles of other throat diameter was similar, making their detailed discussion here superfluous. The most important resulting parameter of the present study was the discharge coefficient C_D. In most experimental studies, including the present one, it was the only reliably measurable parameter in the CFVN. The resulting discharge coefficient C_D as a function of the expression $Re^{-0.5}$ is finally given in Fig. 12. The relationship displayed in Fig. 12 should be linear, as the flow is clearly laminar.

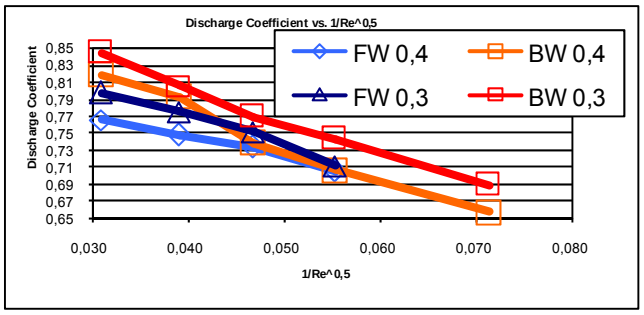

Fig. 12: Discharge coefficient as a function of $Re^{-0.5}$

5. CONCLUSIONS

The flow fields in several micro-sized nozzles have been successfully simulated. In the few experimentally investigated cases, the general agreement between the numerical flow simulations and the experimental data was quantitatively good, showing the correct tendencies. At low pressure ratios (here, p_{out}/p_0 = 0.3), the flow in the throat remained critical at all times. At higher pressure ratios, a premature unchoking was observed. The flow was always unsteady, although the fluctuations displayed in some cases very small amplitudes at very high frequencies. For details, the reader is referred to the original publication of Allofs [8]. The execution of the simulations was rather difficult, as the very strong flow variable gradients at the sharp corners of the nozzles required very high computational grid resolution.

6. REFERENCES

[1] DIN EN ISO 9300:1995, 04.1995: Durchflussmessung von Gasen mit Venturi düsen bei kritischer Strömung.

[2] E. von Lavante, R. Kramer, B. Mickan: "Flow Behaviour in Sonic Micro Nozzles", , Proceedings of Flomeko 2003, Groningen, Netherlands, Mai 2003.

[3] Nakao, Shin-ichi, "Choking Phenomenon of Sonic Venturi Nozzles on Low Reynolds Numbers", Proceedings of the 9th Int. Conference on Flow Measurement LOMEKO'98, Lund, 1998.

[4] Wolf, H.; Kramer, R.; Mickan, B. „Mikrodurchfluss – Flussraten im Bereich Mikroliter pro Minute", Sonderdruck. Braunschweig (119, Heft 1). In: *PTB Mitteilungen, 2009*.

[5] Kramer, R., Mickan, B. and Schmidt, R., „The Application of Critical Nozzles in Series for the Determination of Small Flow Rates and the Generation of Gas Mixtures", Proceeding of Flomeko 2010, Taipei, Taiwan, 2010.

[6] Hänel, D., „Molekulare Gasdynamik – Einführung in die kinetische Theorie der Gase und Lattice-Boltzmann-Methoden", Springer Verlag, 2004, page 10.

[7] Zeitz, D., „Entwicklung eines Strömungslösers von kritisch betriebenen Düsen unter Berücksichtigung von

Realgaseffekten“, Dissertation. Universität Essen, Essen 2002.

[8] Allofs, J., „Numerical Simulation of Flow Fields in Critical Flow Micro-Nozzles Used for Flow Metering”, Diplom-Arbeit, Universität Duisburg-Essen, Lehrstuhl für Strömungsmechanik, 2011.

P2/p0=0,4	d	∂m/∂t, ideal	∂m/∂t, num	C_D,exp	C_D, num
FW	25	117,41	81.28	0.662	0,692
	35	230,13	168,94	-	0,734
	50	469,66	351,42	-	0,748
	80	1202,32	920,66	-	0,766
BW	15	42,27	27.78	-	0,657
	25	117,41	81.18	0.670	0,691
	35	230,13	169.88	-	0,738
	50	469,66	372.18	-	0,792
	80	1202,32	984.68	-	0,819
FW dr.	25	117,41	81,29	0.660	0,692
BW dr.	25	117,41	75,46	0.663	0,643

p2/p0=0,3	d	∂m/∂t, ideal	∂m/∂t, num	C_D,exp	C_D, num
FW	25	117,41	83,54	0,664	0,711
	35	230,13	172,89	-	0,751
	50	469,66	364,02	-	0,775
	80	1202,32	958,38	-	0,797
BW	15	42,27	29,13	-	0,689
	25	117,41	87,29	0.676	0,743
	35	230,13	177,10	-	0,770
	50	469,66	378,59	-	0,806
	80	1202,32	1015,28	-	0,844
FW dr.	25	117,41	84,82	0.662	0,722
BW dr.	25	117,41	85,03	0,667	0,724

Table 1: Summary of results